Received: 18 August 2017 | Accepted: 8 October 2018

DOI: 10.1111/jmg.12458

ORIGINAL ARTICLE

WILEY Journal of METAMORPHIC GEOLOGY

REE partitioning between monazite and garnet: Implications for petrochronology

Bradley Hacker | **Andrew Kylander-Clark** | **Robert Holder**

Earth Science, University of California, Santa Barbara, California

Correspondence
Bradley Hacker, Earth Science, University of California, Santa Barbara, CA.
Email: hacker@geol.ucsb.edu

Funding information
UCSB, Grant/Award Number: NSF EAR-1219942

Handling Editor: Michael Brown

Abstract

Rare-earth element and Y partitioning between garnet and monazite was measured in metamorphic rocks from western Norway to provide more confidence in tying monazite U/Th–Pb dates to *P–T* conditions recorded in garnet. A subset of samples has low-Y garnet mantles and low-Y monazite cores that gave Y-partitioning temperatures similar to independently determined metamorphic temperatures. In combination with previously published data, these monazite–garnet pairs have temperature-dependent partitioning of the HREE from Dy to Lu, and nonsystematic partitioning of the LREE from La–Gd. The temperature-dependent partitioning must be considered when using HREE to assess which portions of garnet and monazite might have coexisted, but experiments are needed to place the dependence on a firm footing.

KEYWORDS

garnet, monazite, partitioning, rare-earth elements

1 | INTRODUCTION

One of the reasons that U/Th–Pb dating of monazite is a powerful petrochronology tool is the potential it offers for tying absolute dates to the evolution of coexisting garnet and thereby adding absolute time to a rock *P–T* path. Central to achieving this objective is determining which portion of the garnet coexisted with which portion of the monazite. The first attempt to do this quantitatively was by Pyle, Spear, Rudnick, and McDonough (2001), who calibrated a thermometer based on the partitioning of Y between monazite and garnet in metapelite at 450–700°C. Subsequently, Hermann and Rubatto (2003) and Rubatto, Hermann, and Buick (2006) extended monazite/garnet partitioning coefficients, K_d, to the rare-earth elements (REE) by measuring grains in granulite-facies metapelites (Figure 1). The authors used mineral textures, mineral compositions and U/Th–Pb zircon and monazite dates to decide which of the several monazite and garnet compositions co-crystallized. Three subsequent studies (Figure 1) have reported coexisting monazite and garnet in granulite- and amphibolite-facies metapelite (Buick, Hermann, Williams, Gibson, & Rubatto, 2006; Mottram et al., 2014; Warren et al., 2018) and generated compositional pairs with K_d values similar to those reported by Hermann and Rubatto (2003) and Rubatto et al. (2006). Unlike the temperature dependence demonstrated for Y partitioning, however, no temperature dependence for HREE partitioning has been recognized. Warren et al. (2018) demonstrated that without knowledge of the temperature-dependent partitioning, the ability to interpret REE partitioning between monazite and garnet is severely limited.

This paper builds on these earlier studies by integrating data from garnet+monazite-bearing rocks from Norway with data from previous studies. The objective of this study is twofold: to (a) measure the partitioning of trace elements in a range of natural monazite and garnet compositions over a range of temperature and (b) demonstrate the temperature dependence of HREE partitioning. The principal finding is that Dy to Lu partitioning between monazite and garnet is temperature dependent—just like Y—and this must be taken into account when using said partitioning to interpret rock history.

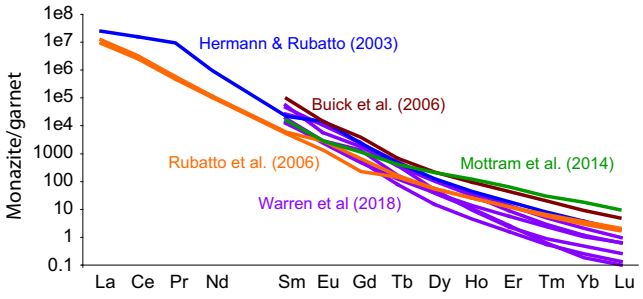

FIGURE 1 Monazite–garnet REE partitioning reported by Hermann and Rubatto (2003), Buick et al. (2006), Rubatto et al. (2006), Mottram et al. (2014), and Warren et al. (2018). *Y*-axis is a dimensionless ratio

2 | DATA COLLECTION

The elemental compositions of monazite and garnet were measured using laser ablation inductively coupled plasma mass spectrometry (LA-ICP-MS) and electron-probe microanalysis (EPMA). Zoning in monazite was qualitatively assessed with X-ray maps created by EPMA and measured quantitatively with LA-ICP-MS spot maps. The LA-ICP-MS and EPMA analytical protocols and data-reduction strategies for monazite are presented in Hacker, Kelemen, and Behn (2015) and Holder, Hacker, Kylander-Clark, and Cottle (2015), and data from those studies are reprised here. Zoning in the largest garnet grains was measured quantitatively with LA-ICP-MS rim–core–rim line scans and EPMA line scans. A Photon Machines 193 nm excimer laser and HelEx sample cell were used, and data were collected on an Agilent 7700S quadrupole ICP-MS; the analyses were obtained with a 50 μm laser spot, using a frequency of 8 Hz, a 25 s ablation time, and an ablation rate of ~100 nm/pulse. Analyses of NIST 612 glass and the basalt standard BHVO-2 (Jochum et al., 2007) were interleaved with the unknowns as reference materials. Data were processed using Iolite version 2.5 (Paton, Hellstrom, Paul, Woodhead, & Hergt, 2011), which corrects for machine drift using NIST 612 as a reference material. The basalt standard BHVO-2 was used as the reference material for all elemental abundances other than Y; Si was used as an internal standard, and the Si content was set to 18 wt%. The Y values calculated by this method are systematically elevated relative to EPMA measurements, so NIST-612 was used to calculate *Y* abundances instead.

EPMA data collection was limited to X-ray maps of a few garnet crystals, and line scan of one garnet. Characteristic-X-ray intensities were measured using WDS and EDS concomitantly. The line scan was collected at 20 kV with a 100 nA beam current and with the beam defocused to a 5 μm diameter spot. The Y Lα intensity was measured using the aggregate WDS intensity measurements from two LPET and one PET analysing crystals. The on-peak count time was 120 s (aggregate 360 s) and the off-peak background count times were 60 s (aggregate 180 s) on both sides of the peak position. All other elemental concentrations were measured using EDS-derived Kα X-ray intensities and quantified by comparison to a reference standard (A99 USNM 113498-1; Jarosewich, Nelen, & Norberg, 1980).

Data are summarized in Table S1; some of these compositions and all the sample locations are presented in Hacker et al. (2015) and Holder et al. (2015). The garnet data were filtered for the presence of zircon, rutile, monazite, apatite, mica, and plagioclase inclusions using Zr, Ti, Ce, P, K, and Sr abundances. The monazite data were filtered for zircon and rutile in the same manner and for the presence of quartz by removing data that yielded nonstoichiometric monazite analyses.

3 | METAMORPHIC HISTORY OF THE STUDY AREA

The Western Gneiss region experienced Precambrian granulite-facies metamorphism, 460–425 Ma Barrovian metamorphism progressing to 425–405 Ma eclogite facies metamorphism at up to 3.6 GPa (Cuthbert, Carswell, Krogh-Ravna, & Wain, 2000), and then near-isothermal decompression to 0.5–1.0 GPa during amphibolite facies metamorphism at *c.* 400–380 Ma (Hacker et al., 2015; Holder et al., 2015; Kylander-Clark & Hacker, 2014; Labrousse et al., 2004; Root et al., 2005; Walsh & Hacker, 2004). This late amphibolite facies overprint occurred at 650–775°C (Garber, Hacker, Kylander-Clark, Stearns, & Seward, 2017). All the samples in this study are pelitic or quartzofeldspathic, and contain apatite; one (E9804J1) contains xenotime and two (E9814A5, E1614C) contain allanite (see descriptions in Hacker et al., 2015; Holder et al., 2015).

FIGURE 2 Garnet REE compositions, garnet zoning, and monazite REE compositions. At least two garnet grains were measured in each sample; shown is the garnet with the most-complete record. Garnet and monazite REE compositions are shown separately for grain cores (red), mantles (green), and rims (blue); the equivalent domains in garnet are indicated in the zoning profiles with pale red, pale green, and pale blue. In the "garnet REE" columns, the apparent Y-MG temperatures for cores, mantles, and rims are given in red, green, and blue. Garnet core, mantle and rim compositions presented in Table S1 are indicated with vertical lines. In the "monazite REE" columns, a yttrium X-ray map demonstrates the zoning

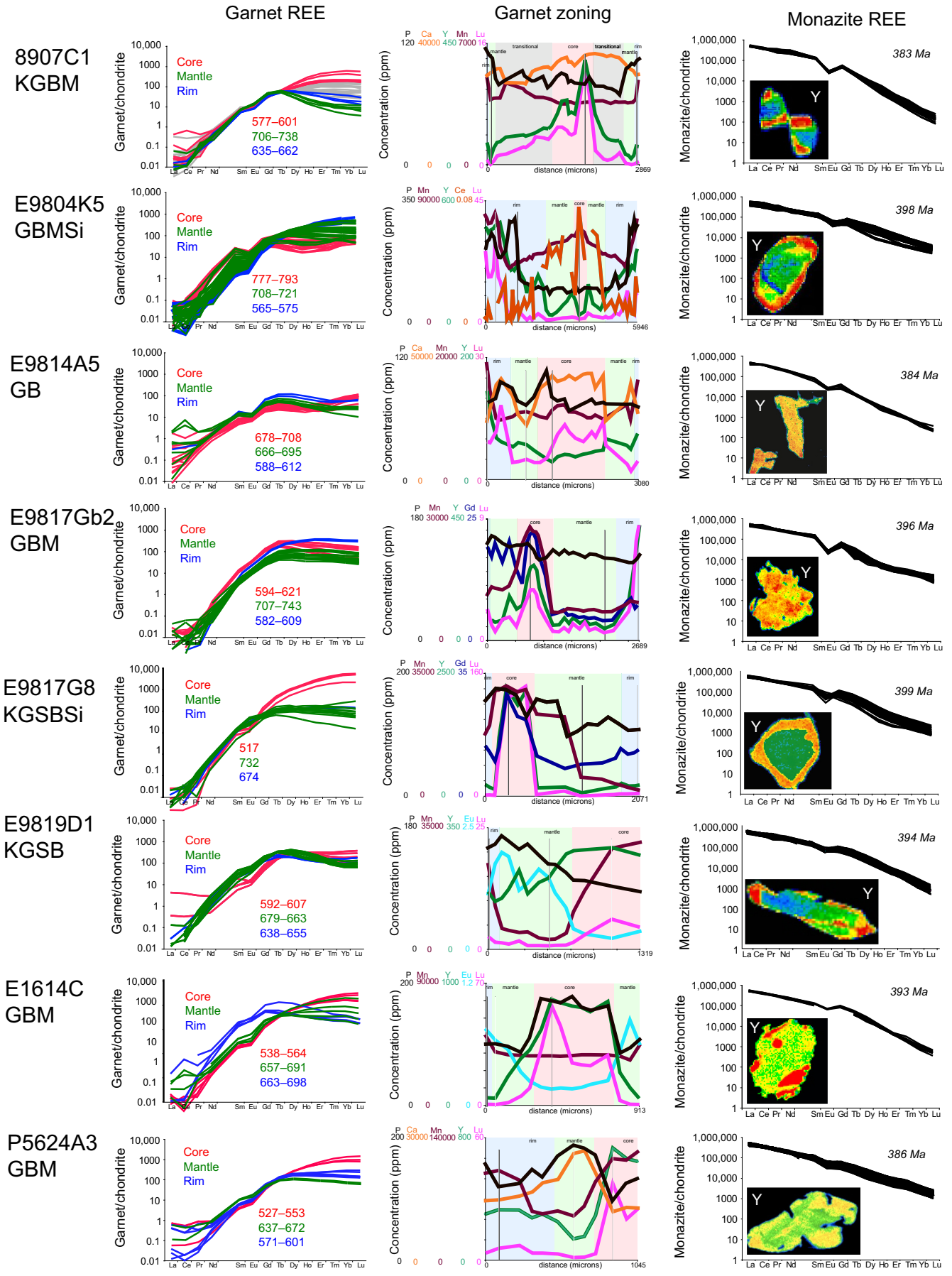
Garnet REE
Garnet zoning
Monazite REE
8907C1
KGBM
Core
Mantle
Rim
577–601
706–738
635–662
383 Ma
E9804K5
GBMSi
777–793
708–721
565–575
398 Ma
E9814A5
GB
678–708
666–695
588–612
384 Ma
E9817Gb2
GBM
594–621
707–743
582–609
396 Ma
E9817G8
KGSBSi
517
732
674
399 Ma
E9819D1
KGSB
592–607
679–663
638–655
394 Ma
E1614C
GBM
538–564
657–691
663–698
393 Ma
P5624A3
GBM
527–553
637–672
571–601
386 Ma
Garnet/chondrite
Concentration (ppm)
Monazite/chondrite
distance (microns)

The garnet in the study area had a complicated history. Some grew during Precambrian granulite facies metamorphism, others grew or recrystallized during the 440–405 Ma subduction related metamorphism, and others during the *c.* 400–390 Ma amphibolite facies metamorphism; all garnet then underwent partial resorption driven by further cooling and/or decompression (Peterman, Hacker, & Baxter, 2009; Root et al., 2005; Walsh & Hacker, 2004). This resorption is evident in the rounded, embayed grain habits, and in the increases in compatible-element (e.g., Mn and Y) concentrations in the grain rims (see below).

The monazite in the study area experienced a recrystallization history similar to that of the garnet, and records U–Pb dates of *c.* 1.6 and 0.9 Ga related to granulite facies metamorphism, 460–405 Ma reflecting collisional/subduction events, and 400–380 Ma related to the late amphibolite facies overprint (Hacker et al., 2015; Holder et al., 2015). This study is restricted to less-complicated monazite that is dated at 399–383 Ma. Based on protolith ages and the local preservation of older dates in some monazite, it is likely that the monazite investigated in this study grew during one of the earlier metamorphic episodes, and then thoroughly recrystallized during the final amphibolite facies event at 650–775°C (Hacker et al., 2015; Holder et al., 2015).

4 | RESULTS

4.1 | Reaction relationship between garnet and monazite

The rocks in this study contain 5–25% garnet, plus plagioclase, apatite, mica, quartz, <0.1% monazite; they generally lack xenotime and allanite. Kyanite (seven samples), sillimanite (six) and/or staurolite (two) are present (Figure 2 lists the AKFM assemblage for each sample). As a result, the net-transfer reaction

$$\begin{aligned} &Y_3Al_2Al_3O_{12}(\text{YA-garnet}) + Ca_5(PO_4)_3(OH)(\text{OH-apatite}) \\ &\quad + {}^{25/4}\,SiO_2 = {}^{5/4}\,Ca_3Al_2Si_3O_{12}(\text{Ca-garnet}) \\ &\quad + {}^{5/4}\,CaAl_2Si_2O_8(\text{Ca-plagioclase}) \\ &\quad + 3YPO_4(\text{Y-monazite}) + {}^{1/2}\,H_2O \end{aligned} \quad (1)$$

of Pyle et al. (2001) is likely a fair description of the subsolidus P+Y+HREE transfer that occurred when these minerals were stable. There are at least two exceptions to this simplistic description. (a) Relict eclogite within amphibolite facies gneiss reveals that most of the study area reached pressures where plagioclase was unstable (Labrousse et al., 2004; Root et al., 2005; Walsh & Hacker, 2004); monazite in a few samples recorded this event in elevated Sr and Eu abundances and subduction-related dates (Holder et al., 2015). At those elevated pressures, P+Y+HREE partitioning between monazite and garnet would have involved other minerals—chiefly clinopyroxene; we mitigate this complication by excluding such monazite from consideration. (b) Above the solidus, monazite stability is reduced by the phosphorus solubility in silicate liquid, whereas garnet abundance may increase or decrease (Auzanneau, Vielzeuf, & Schmidt, 2006; Kelsey, Clark, & Hand, 2008; Stepanov, Hermann, Rubatto, & Rapp, 2012); we mitigate this complication by excluding samples that reached temperatures above 725–750°C. The ages, textures, and compositions of minerals in the remaining samples are compatible with the coexistence of garnet and monazite.

Reaction 1 dictates that, at subsolidus conditions, the Y and HREE concentrations of the garnet and monazite were controlled by the compositions of those minerals, the bulk composition of the rock, and the ambient pressure and temperature (Pyle et al., 2001; Spear & Pyle, 2010). In the garnet+biotite+aluminumsilicate±staurolite stability fields—typical of the present sample suite—increasing pressure and/or decreasing temperature causes growth of garnet and consumption of monazite, and the Y content of both is predicted to decrease; decreasing pressure and/or increasing temperature causes the opposite (Spear & Pyle, 2010). The ratio of Y in monazite to Y in garnet in the studied rocks varies from 10 to 1,000 (Table S1), comparable to the inverse ratios of the modes of these minerals, such that changes in garnet abundance likely strongly affected the composition of monazite (Spear & Pyle, 2010); for example, garnet decomposition could have driven the uptake of Y by monazite.

The stability, abundance, and composition of monazite are affected by the availability of phosphorus and LREE. Hydroxyl-apatite contains 185,000 ppm P, monazite has 130,000 ppm P, and garnet in this study stores <100 ppm P (Table S1). Hydroxyl-apatite typically contains <500 ppm Ce, monazite in this study ~240,000 ppm Ce, and garnet has 0.01–0.2 ppm Ce. These compositions indicate that the (a) decomposition of apatite releases significant P, increasing the monazite mode, and diluting the abundance of Y in monazite (and garnet if it remains in equilibrium); (b) release of Ce from apatite can have only a minor effect on monazite mode and composition, but can cause an uptick in garnet Ce content; (c) decomposition of garnet releases insignificant P and Ce such that the mode of monazite will change little in response (Spear & Pyle, 2010); decomposition of monazite releases significant P and Ce that can stimulate apatite production, and may cause a recognizable increase in those elements in garnet.

4.2 | Zoning

All the garnet in the sample suite is zoned (Figure 2). We divided each garnet into three zones: core, mantle and rim. In Figure 2, these zones are depicted with red, green, and

blue lines in the "garnet REE" columns and pale red, pale green, and pale blue regions in the "garnet zoning" columns. The boundaries between these zones range from sharp to gradational and, for different elements, may lie in different locations in the garnet—likely because of differences in element mobility—and this leads to some ambiguity in defining the zones. Generally, we chose the rim/mantle boundary based on changes in Y+HREE abundances—an alternative definition, based on e.g., Mn, is possible, but this study focuses on Y+REE.

All the garnet grains, except one (E9804K5), have core-to-mantle decreases in Y+HREE±Mn abundances that are compatible with Rayleigh-type fractionation of Y+HREE during garnet growth (Hollister, 1966); E9804K5 garnet (Figure 2) lacks a core peak in HREE, which could be the result of diffusional homogenization or a section not passing through the garnet core. All the garnet grains have HREE±Mn increases at the rims. Zoning like this is typical of Western Gneiss region garnet (Root et al., 2005; Walsh & Hacker, 2004). Figure 3 shows that the rimward enrichment in the HREE depends on ionic size, and is mirrored by LREE loss. This type of zoning is compatible with more extreme garnet resorption, loss of LREE, retention of HREE, and diffusion of REE. The lengthscale of the rimward REE increase in garnet cannot be measured more precisely than the 50 μm size of the laser spots, but is a few hundred microns in most garnet.

The 50 μm spot size of the laser means that finer scale compositional zoning is not resolved. As an example, the EPMA line scan (Figure 4) demonstrates that the rim zoning in garnet from sample R9823A2—wherein the Y concentration reaches >250 ppm within 10 μm of the rim—is badly aliased by the ICP spots measurements that peak at only 92 ppm. Such aliasing must be considered when interpreting garnet–monazite element partitioning measured by ICP.

The interpretation that the Y+HREE±Mn increases at the garnet rims resulted from resorption follows that of several previous studies (e.g., Kelly, Carlson, & Connelly, 2011; Kohn, 2009; Kohn & Malloy, 2004). The alternative —that the increases in Y+HREE±Mn were caused by the breakdown of other HREE-bearing phases during garnet growth (Konrad-Schmolke, Zack, O'Brien, & Jacob, 2008; Spear & Pyle, 2010)—is unlikely for three reasons: (a) Allanite may be involved in the growth of monazite at lower amphibolite facies temperatures (Spear, 2010), but it incorporates more LREE than HREE, opposite to the zoning in E9804K5 (Figure 3). (b) Xenotime may also be involved in the growth of monazite at amphibolite facies temperatures (Spear & Pyle, 2010) and has a garnet-like preference for the HREE over LREE, but it does not take up significant Mn. (c) Allanite and xenotime are present in only three samples, and the garnet zoning in those samples is similar to that in the other samples.

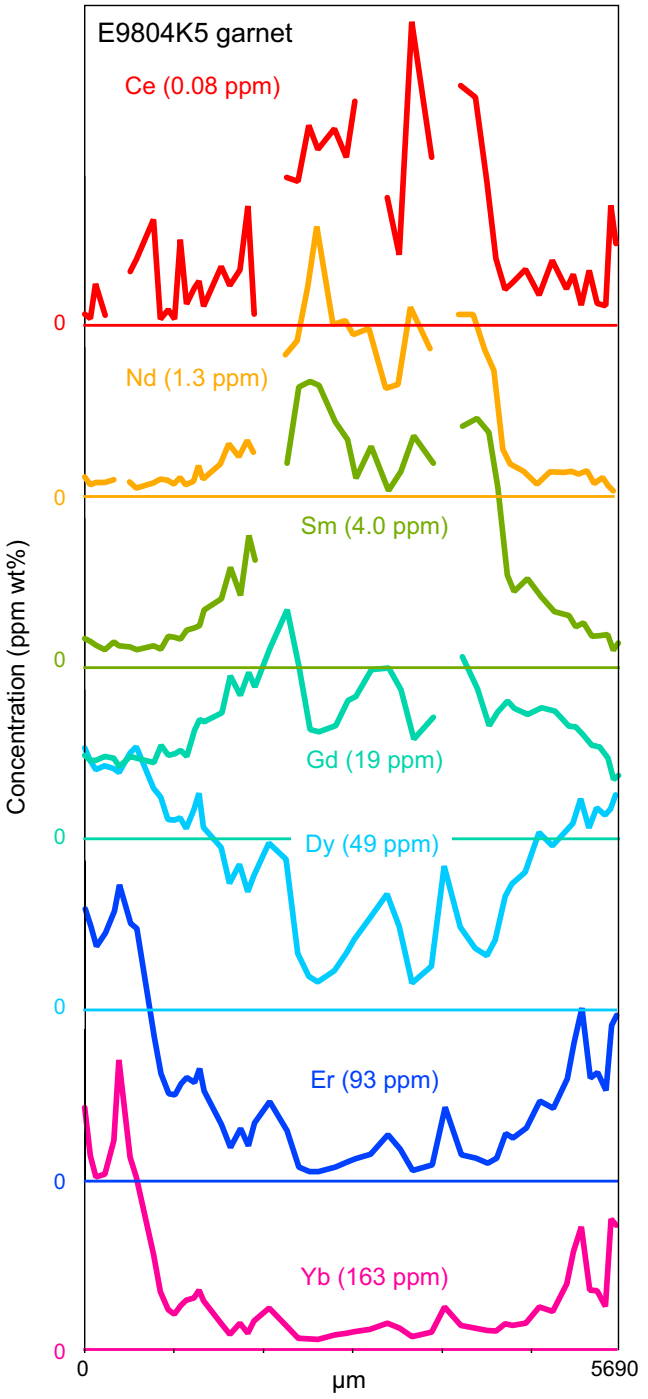

FIGURE 3 Rim-core-rim zoning in garnet from sample E9804K5 shows that rimward enrichment in HREE depends on ionic size, and is mirrored by rimward LREE loss. Maximum values shown in parentheses

Most of the monazite in the sample suite has HREE-rich rims. In most samples this zoning spans less than a factor-of-2 variation (black lines in the "monazite REE" column of Figure 2). Many other samples examined have more extreme zoning and were excluded from consideration. For additional information about the

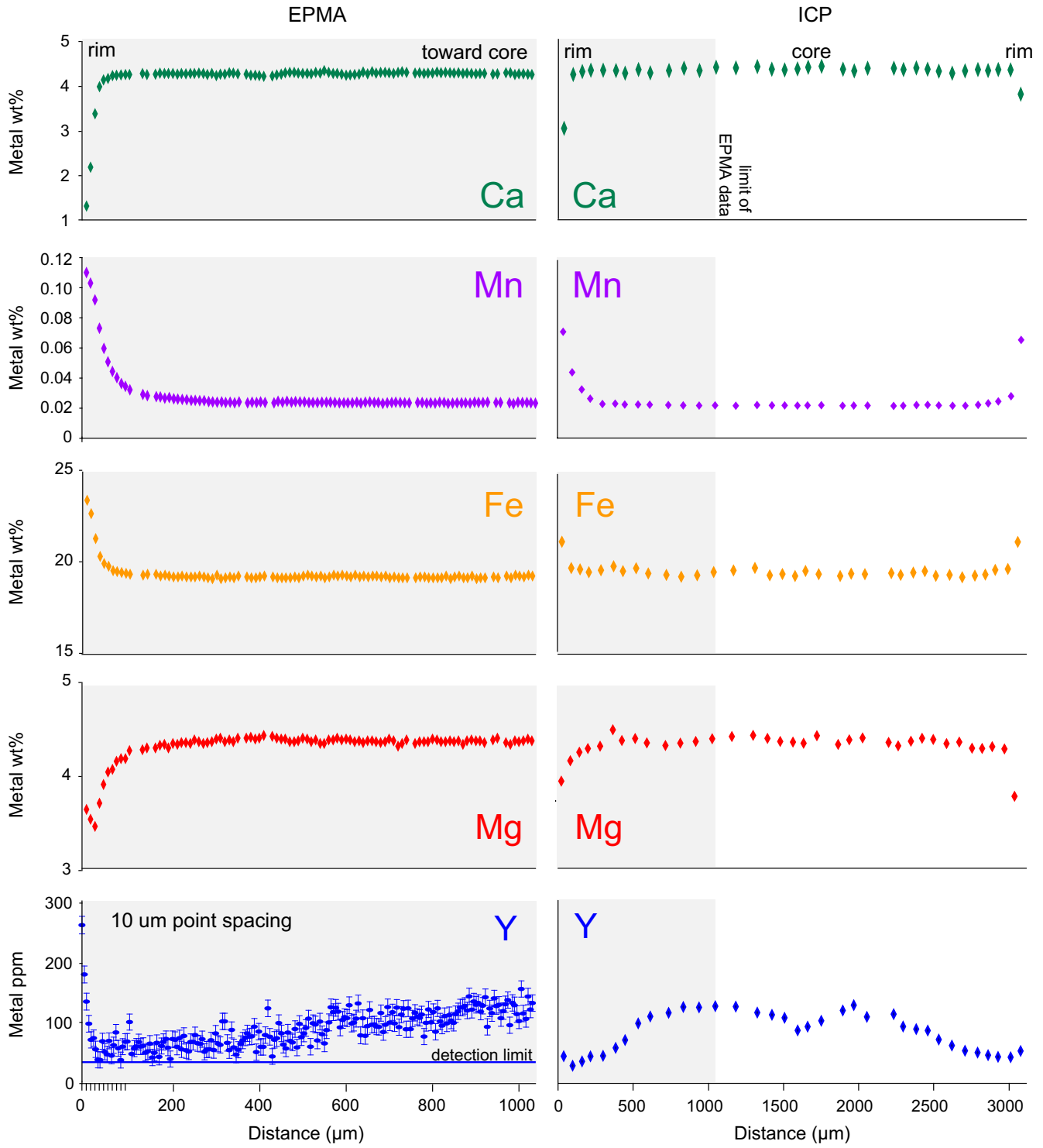

FIGURE 4 Zoning in garnet (sample R9823A2), demonstrating aliasing produced by 50 μm ICP laser spots relative to 10 μm EPMA spots; grey background shows area of overlap of EPMA and ICP data

monazite, see Hacker et al. (2015) and Holder et al. (2015).

The preservation of REE zoning in garnet and monazite is expected. The lengthscale for Dy diffusion in garnet for 10 Ma at 800°C is ~30–70 μm (Carlson, 2012; Van Orman, Grove, Shimizu, & Layer, 2002); the rimward increases in HREE in most garnet grains in Figure 2 are within an order of magnitude of this estimate. Although REE diffusion in monazite has not been measured experimentally, the characteristic lengthscale for Dy diffusion in xenotime for 10 Ma at 800°C is far less: 0.03–0.2 μm (Cherniak, 2006).

5 | INTERPRETATION

The observations and discussion above lead to the expectation that the Y-rich garnet rims and Y-rich monazite rims developed during partial resorption of the garnet. The back diffusion of Y into garnet and the aliasing of the near-rim gradient in Y composition produced by the 50 μm laser spots make use of these data problematic. Prior to resorption, however, the low-Y part of the garnet—now perhaps preserved in the garnet mantle—likely coexisted with the low-Y monazite. If this is correct, comparing REE partitioning between the low-Y garnet and the low-Y monazite may be possible.

The apparent temperature for all two dozen samples in the data set were calculated using the Y monazite–garnet (Y-MG) thermometer of Pyle et al. (2001) (Figure 5a) and compared that to the metamorphic temperature of the rock determined independently from other thermobarometers (Root et al., 2005; Spencer et al., 2013; Walsh & Hacker, 2004; Table S1). We rejected from consideration all samples for which the temperature difference is ≥100°C. The remaining eight samples are depicted in Figure 2 and in red in Figure 5a, in which the calculated Y-MG temperature is plotted against the logarithm of the activity product ratio, K_{eq} crafted by Pyle et al. (2001):

$$K_{eq} = \frac{X_{Ca-garnet}^{15/4} X_{Ca-plagioclase}^{5/4} X_{Y-monazite}^{3} f_{H_2O}^{1/2}}{X_{Y-garnet}^{3} X_{OH-apatite}}$$

based on Reaction 1, above. We did not measure the OH content of apatite in the samples, and choose X_{OH}-apatite = 0.2 after Pyle et al. (2001); this is a minor simplification as 100% uncertainty in this value causes <15°C difference in temperature. Plagioclase in the samples is typically oligoclase (Root et al., 2005; Walsh & Hacker, 2004); $X_{an} = 0.25$ was used for all samples, noting that X_{an} in the range 0.15–0.35 yields temperatures that differ by <10°C. We chose a pressure of 1 GPa and calculated H_2O fugacity using Pitzer and Sterner (1994), assuming $x_{H_2O} = 1$; for the range of independent temperature estimates, plausible differences in $f_{H_2O}^{1GPa}$ result in <5°C difference in Y-MG temperatures, but if the pressure was really 2 GPa, the calculated temperatures are ~25°C too high. The Y was not measured in some monazite; for these samples Y was calculated using the average Y/Ho ratio from other samples in this study (24 ± 2). The Y uptake in monazite is influenced by Th uptake (Seydoux-Guillaume, Wirth, Heinrich, & Montel, 2002), but the bulk of the monazite in this study has <3 mol.% $ThSiO_4$, so the effect is expected to be <30°C for the cases considered herein. Pressure has a smaller effect on garnet REE fractionation than temperature (Moretti & Ottonello, 1998), but whether this is true for monazite remains unknown. In summary, the effect of these considerations on the Y-MG temperature is less than our 100°C rejection criterion.

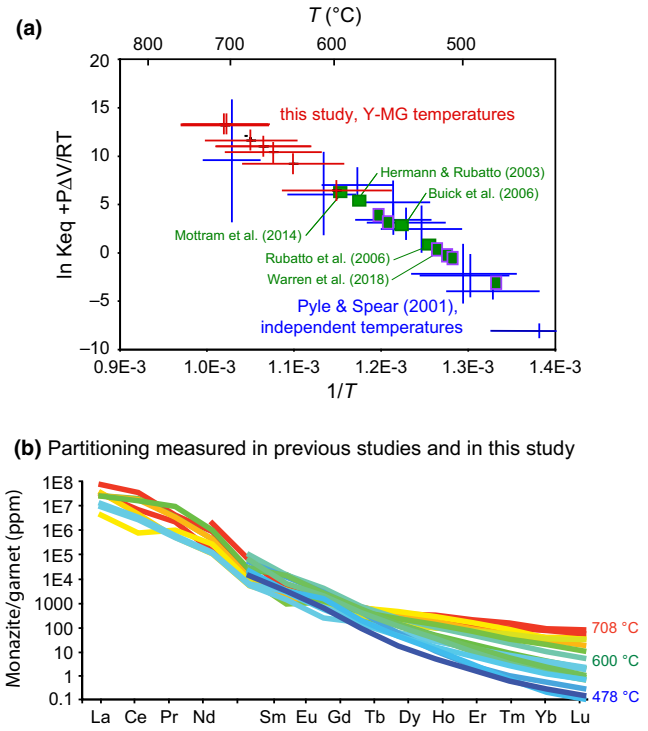

FIGURE 5 (a) Y-MG temperature versus ln K_{eq} of Equation 1. Blue: ln K_{eq}–T data from Pyle et al. (2001) used to define the fit for the Y-MG thermobarometer; temperatures for each datum were determined independently as described by Pyle and Spear (2000). Two of the ln K_{eq} values in the original publication were corrected in consultation with F. Spear. Red: ln K_{eq}–T data from this study with calculated Y-MG temperatures that are within 100°C of independently determined temperature. Uncertainties include variations of 10% in Y and X_{An}, 50% in ap-OH, and 1 GPa in pressure and H_2O fugacity. Green: ln K_{eq}-Y-MG temperatures calculated from monazite–garnet pairs presented in other studies. (b) There is a clear dependence of garnet–monazite HREE partitioning measured in this and previous studies on Y-MG temperature; warm/cold colours show samples with high/low Y-MG temperatures

In Figure 5a, the data in blue are those used by Pyle et al. (2001) to determine ΔH, ΔS, and ΔV for the thermometer. In green are the Y-MG temperatures calculated from data presented in previous studies. The Y-MG for the monazite–garnet pair presented by Mottram et al. (2014) is within 100°C of the independently determined temperature of 650°C, but the Y values reported by Hermann and Rubatto (2003), Rubatto et al. (2006), and Buick et al. (2006) yield Y-MG temperatures of 518–580°C (Table S1), more than 200°C different than the metamorphic temperatures of 800–825°C inferred for those rocks from independent means. Three of the samples analysed by Warren et al. (2018) are within 100°C of the expected value, and three are not.

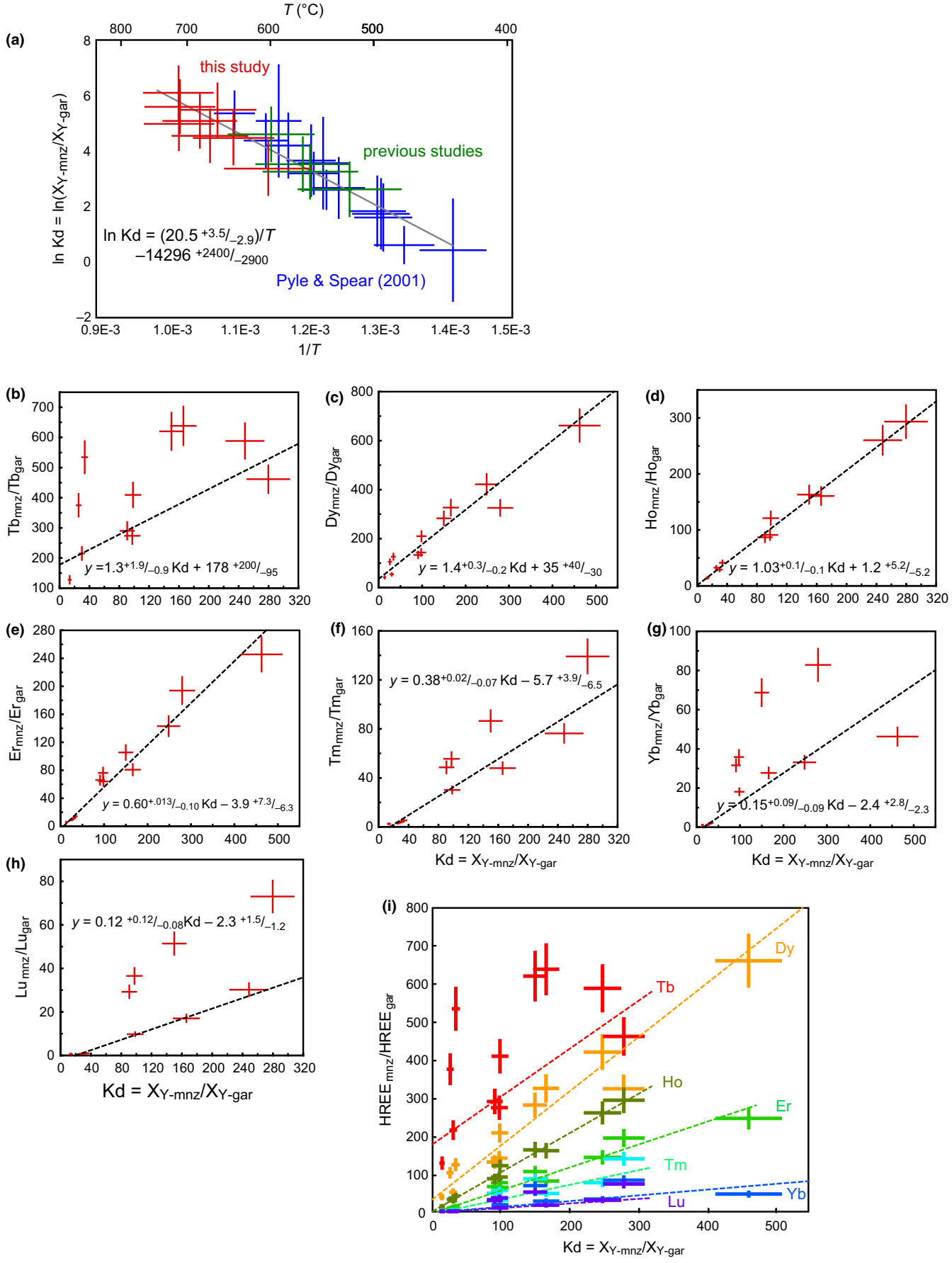
(a)
T (°C)
800 700 600 500 400
this study
previous studies
Pyle & Spear (2001)
ln Kd = (20.5 +3.5/–2.9)/T
–14296 +2400/–2900
ln Kd = ln(XY-mnz/XY-gar)
1/T
0.9E-3 1.0E-3 1.1E-3 1.2E-3 1.3E-3 1.4E-3 1.5E-3
(b)
Tbmnz/Tbgar
y =1.3+1.9/–0.9 Kd + 178 +200/–95
(c)
Dymnz/Dygar
y = 1.4+0.3/–0.2 Kd + 35 +40/–30
(d)
Homnz/Hogar
y = 1.03+0.1/–0.1 Kd + 1.2 +5.2/–5.2
(e)
Ermnz/Ergar
y = 0.60+.013/–0.10 Kd – 3.9 +7.3/–6.3
(f)
Tmmnz/Tmgar
y = 0.38+0.02/–0.07 Kd – 5.7 +3.9/–6.5
(g)
Ybmnz/Ybgar
y = 0.15+0.09/–0.09 Kd – 2.4 +2.8/–2.3
Kd = XY-mnz/XY-gar
(h)
Lu mnz/Lugar
y = 0.12 +0.12/–0.08Kd – 2.3 +1.5/–1.2
Kd = XY-mnz/XY-gar
(i)
HREE mnz/HREE gar
Dy
Tb
Ho
Er
Tm
Lu
Yb
Kd = XY-mnz/XY-gar

FIGURE 6 (a) Y-MG temperature versus ln K_d of Equation 2 for the data in Figure 5a. Temperature uncertainty assumed to be ±50°C, and ln K_d uncertainty determined as the average percentage difference between the true ln K_{eq} value and the ln K_{eq} value calculated assuming $X_{grs} = 0.1$, $X_{an} = 0.25$, $X_{OH\text{-}apatite} = 0.2$, $p = 1$ GPa, f_{H_2O}=1.4448 GPa (see text). The fit shown is from the robust regression function of Isoplot (Ludwig, 2003). (b–h) Relationships between monazite/garnet element partitioning and Y-MG temperature. *X*-axes are Y-MG temperature (Pyle et al., 2001), and *Y*-axes are the elemental partitioning between monazite and garnet expressed as a ppm ratio. Temperature uncertainty assumed to be ±50°C, and ratio uncertainty assumed to be 10%. The dependences are fit using the robust regression function of Isoplot (Ludwig, 2003) (i) Same data as (b–h) plotted to the same scale and coloured by element

6 | TEMPERATURE-DEPENDENT PARTITIONING

The temperature-dependent partitioning evident in Y should be present in the HREE, as suggested by Warren et al. (2018). This is evident in Figure 5b, which shows the monazite/garnet REE partitioning reported by Hermann and Rubatto (2003), Rubatto et al. (2006), Buick et al. (2006), Warren et al. (2018), and this study, coloured by Y-MG temperature.

We explore the temperature dependence of HREE partitioning by examining the relationship between HREE partitioning and Y partitioning in Figure 6a–i. Because many petrochronology studies of monazite–garnet element partitioning do not measure plagioclase composition, apatite composition, and/or determine f_{O_2}—partly because of the modest effect these variables have on Y-MG—we replot in Figure 6a the data of Figure 5a in a simplified form that depends only on the Y contents (ppm) of garnet and monazite:

$$K_d = \frac{X_{\mathrm{Y-monazite}}}{X_{\mathrm{Y-garnet}}} \quad (2)$$

The relationship between temperature and monazite–garnet Y partitioning is still preserved (Figure 6a), albeit with less accuracy and precision. The HREE from Tb to Lu also show clear partitioning by monazite and garnet (Figure 6b–i). These relationships are quantified as correlations between $HREE_{mnz}/HREE_{gar}$ and Y_{mnz}/Y_{gar}. The value in displaying the data this way—rather than as $HREE_{mnz}/HREE_{gar}$ versus temperature—is that even if the temperatures are systematically incorrect, the variation in the HREE with respect to Y is unchanged. The fit is best for Ho (Figure 6d), the HREE closest in ionic radius to Y. The fit degrades for ions both larger and smaller than Ho, and is particularly poor for Tb, Yb, and Lu. This degradation could result from (a) a nonlinear dependence of partitioning, (b) inclusion of monazite and garnet that did not co-crystallize, or (c) inaccurate measurements of trace-element abundances. As noted below, experiments are likely required to place the temperature dependence on a firm footing. The LREE—La through Gd—do not show a linear relationship with Y-MG temperature or Y_{mnz}/Y_{gar} because the LREEs are essential structural constituents in monazite (Hanson & Langmuir, 1978); the partitioning of these elements between monazite and garnet is constant in the present data set within the uncertainty of the measurements.

The temperature dependence of monazite–garnet HREE partitioning quantified by the fits in Figure 6 is shown graphically in Figure 7, and provides a systematic explanation for the variation in partitioning seen in this and previous studies (Figure 5a). The implication is that monazite–garnet pairs formed at different temperatures should have HREE partitioning that varies by two to three orders of magnitude. For example, pairs formed at ~800°C should have K_d values of ~100–1,000 for all HREE, whereas pairs formed at 500°C should have K_d values that range from ~1,000 (Tb) to <1 (Lu) with decreasing ionic radius.

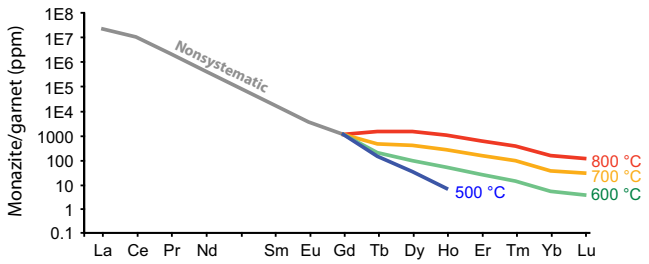

FIGURE 7 Temperature dependent monazite–garnet HREE partitioning calculated from Y-HREE relationships in Figure 6

7 | FUTURE WORK

Experiments have been conducted to measure REE partitioning between garnet and zircon (see summary in Taylor et al., 2017), and this has enabled increasingly meaningful application to natural rocks. Similar experiments to measure REE partitioning between garnet and monazite would be a welcome advance. Until such experiments are completed, the identification of co-crystallized monazite and garnet is best done with Y partitioning rather than HREE partitioning.

8 | CONCLUSION

Monazite and garnet coexist in rocks across a metamorphic field gradient in the Western Gneiss region of Norway.

Partial garnet breakdown produced Y-rich rims on garnet and monazite. When garnet was stable, Y-poor compositions preserved in the garnet mantle are likely to have coexisted with Y-poor monazite. Some of these Y-poor garnet–monazite pairs have the Y partitioning that is expected for their different metamorphic temperatures. These same monazite–garnet pairs, along with other empirical and experimental monazite-garnet pairs from the literature, also define temperature-dependent partitioning for the HREE. The use of HREE partitioning between garnet and monazite to assess which garnet and monazite coexisted—a method commonly used to infer the *P–T* conditions of monazite (re)crystallization—must take this temperature dependence into account. Experiments to quantify the temperature dependence of monazite–garnet REE partitioning are encouraged.

ACKNOWLEDGMENTS

This study was funded by UCSB and NSF EAR-1219942. F. Spear help clarify some of the data in Pyle et al. (2001). He, C. Clark, and an anonymous reviewer provided reviews that resulted in substantial improvement of the manuscript.

ORCID

Bradley Hacker http://orcid.org/0000-0003-2732-1712
Robert Holder http://orcid.org/0000-0002-1119-6905

REFERENCES

Auzanneau, E., Vielzeuf, D., & Schmidt, M. W. (2006). Experimental evidence of decompression melting during exhumation of subducted continental crust. *Contributions to Mineralogy and Petrology*, *152*, 125–148. https://doi.org/10.1007/s00410-006-0104-5

Buick, I. S., Hermann, J., Williams, I. S., Gibson, R. L., & Rubatto, D. (2006). A SHRIMP U–Pb and LA-ICP-MS trace element study of the petrogenesis of garnet–cordierite–orthoamphibole gneisses from the Central Zone of the Limpopo Belt, South Africa. *Lithos*, *88*, 150–172. https://doi.org/10.1016/j.lithos.2005.09.001

Carlson, W. D. (2012). Rates and mechanism of Y, REE, and Cr diffusion in garnet. *American Mineralogist*, *97*, 1598–1618. https://doi.org/10.2138/am.2012.4108

Cherniak, D. (2006). Pb and rare earth element diffusion in xenotime. *Lithos*, *88*, 1–14. https://doi.org/10.1016/j.lithos.2005.08.002

Cuthbert, S. J., Carswell, D. A., Krogh-Ravna, E. J., & Wain, A. (2000). Eclogites and eclogites in the Western Gneiss Region, Norwegian Caledonides. *Lithos*, *52*, 165–195. https://doi.org/10.1016/S0024-4937(99)00090-0

Garber, J., Hacker, B., Kylander-Clark, A., Stearns, M., & Seward, G. (2017). Controls on trace element uptake in metamorphic titanite: Implications for petrochronology. *Journal of Petrology*, *58*, 1031–1057. https://doi.org/10.1093/petrology/egx046

Hacker, B. R., Kelemen, P. B., & Behn, M. D. (2015). Continental lower crust. *Annual Review of Earth and Planetary Sciences*, *43*, 167–205.

Hanson, G. N., & Langmuir, C. H. (1978). Modelling of major elements in mantle-melt systems using trace element approaches. *Geochimica et Cosmochimica Acta*, *42*, 725–741. https://doi.org/10.1016/0016-7037(78)90090-X

Hermann, J., & Rubatto, D. (2003). Relating zircon and monazite domains to garnet growth zones: Age and duration of granulite facies metamorphism in the Val Malenco lower crust. *Journal of Metamorphic Geology*, *21*, 833–852. https://doi.org/10.1046/j.1525-1314.2003.00484.x

Holder, R., Hacker, B., Kylander-Clark, A., & Cottle, J. (2015). Monazite trace-element and isotopic signatures of (ultra)high-pressure metamorphism: Examples from the Western Gneiss Region, Norway. *Chemical Geology*, *409*, 99–111. https://doi.org/10.1016/j.chemgeo.2015.04.021

Hollister, L. S. (1966). Garnet zoning: An interpretation based on the Rayleigh fractionation model. *Science*, *154*, 1647–1651. https://doi.org/10.1126/science.154.3757.1647

Jarosewich, E., Nelen, J. A., & Norberg, J. A. (1980). Reference samples for electron microprobe analysis. *Geostandards Newsletter*, *4*, 43–47. https://doi.org/10.1111/j.1751-908X.1980.tb00273.x

Jochum, K. P., Nohl, U., Herwig, K., Lammel, E., Stoll, B., & Hofmann, A. W. (2007). GeoReM: A new geochemical database for reference materials and isotopic standards. *Geostandards and Geoanalytical Research*, *29*, 333–338.

Kelly, E., Carlson, W., & Connelly, J. (2011). Implications of garnet resorption for the Lu–Hf garnet geochronometer: An example from the contact aureole of the Makhavinekh Lake Pluton, Labrador. *Journal of Metamorphic Geology*, *29*, 901–916. https://doi.org/10.1111/j.1525-1314.2011.00946.x

Kelsey, D. E., Clark, C., & Hand, M. (2008). Thermobarometric modelling of zircon and monazite growth in melt-bearing systems: Examples using model metapelitic and metapsammitic granulites. *Journal of Metamorphic Geology*, *26*, 199–212. https://doi.org/10.1111/j.1525-1314.2007.00757.x

Kohn, M. J. (2009). Models of garnet differential geochronology. *Geochimica et Cosmochimica Acta*, *73*, 170–182. https://doi.org/10.1016/j.gca.2008.10.004

Kohn, M. J., & Malloy, M. A. (2004). Formation of monazite via prograde metamorphic reactions among common silicates: Implications for age determinations. *Geochimica et Cosmochimica Acta*, *68*, 101–113. https://doi.org/10.1016/S0016-7037(03)00258-8

Konrad-Schmolke, M., Zack, T., O'Brien, P., & Jacob, D. E. (2008). Combined thermodynamic and rare earth element modelling of garnet growth during subduction: Examples from ultrahigh-pressure eclogite of the Western Gneiss Region, Norway. *Earth and Planetary Science Letters*, *272*, 488–498. https://doi.org/10.1016/j.epsl.2008.05.018

Kylander-Clark, A., & Hacker, B. R. (2014). Age and significance of felsic dikes from the UHP Western Gneiss Region. *Tectonics*, *33*, 2342–2360. https://doi.org/10.1002/2014TC003582

Labrousse, L., Jolivet, L., Andersen, T. B., Agard, P., Maluski, H., & Schärer, U. (2004). Pressure-temperature-time-deformation history of the exhumation of ultra-high pressure rocks in the Western Gneiss region, Norway. In D. L. Whitney, C. Teyssier, & C. S. Siddoway (Eds.), *Gneiss domes in orogeny* (Geological Society of America Special Paper) (pp. 155–185). Denver, CO: Geological Society of America. https://doi.org/10.1130/0-8137-2380-9

Ludwig, K. R. (2003). Isoplot 3.00. A geochronological toolkit for Microsoft Excel. *Berkeley Geochronology Center Special Publication*, *4*.

Moretti, R., & Ottonello, G. (1998). An appraisal of endmember energy and mixing properties of rare earth garnets. *Geochimica et cosmochimica acta*, *62*, 1147–1173. https://doi.org/10.1016/S0016-7037(98)00033-7

Mottram, C. M., Warren, C. J., Regis, D., Roberts, N. M. W., Harris, N. B. W., Argles, T., & Parrish, R. (2014). Developing an inverted Barrovian sequence: Insights from monazite petrochronology. *Earth and Planetary Science Letters*, *403*, 418–431. https://doi.org/10.1016/j.epsl.2014.07.006

Paton, C., Hellstrom, J. C., Paul, B., Woodhead, J. D., & Hergt, J. M. (2011). Iolite: freeware for the visualisation and processing of mass spectrometer data. *Journal of Analytical Atomic Spectrometry*. https://doi.org/10.1039/clja10172b

Peterman, E. M., Hacker, B. R., & Baxter, E. F. (2009). Phase transformations of continental crust during subduction and exhumation: Western Gneiss Region, Norway. *European Journal of Mineralogy*, *21*, 1097–1118. https://doi.org/10.1127/0935-1221/2009/0021-1988

Pitzer, K. S., & Sterner, S. M. (1994). Equations of state valid continuously from zero to extreme pressures for H_2O and CO_2. *Journal of Chemical Physics*, *101*, 3111–3116. https://doi.org/10.1063/1.467624

Pyle, J. M., & Spear, F. S. (2000). An empirical garnet (YAG)-xenotime thermometer. *Contributions to Mineralogy and Petrology*, *138*, 51–58. https://doi.org/10.1007/PL00007662

Pyle, J. M., Spear, F. S., Rudnick, R. L., & McDonough, W. F. (2001). Monazite-xenotime and monazite-garnet equilibrium in metapelites and a new monazite-garnet thermometer. *Journal of Petrology*, *42*, 2083–2117. https://doi.org/10.1093/petrology/42.11.2083

Root, D. B., Hacker, B. R., Gans, P., Eide, E., Ducea, M., & Mosenfelder, J. (2005). Discrete ultrahigh-pressure domains in the Western Gneiss Region, Norway: Implications for formation and exhumation. *Journal of Metamorphic Geology*, *23*, 45–61. https://doi.org/10.1111/j.1525-1314.2005.00561.x

Rubatto, D., Hermann, J., & Buick, I. S. (2006). Temperature and bulk composition control on the growth of monazite and zircon during low-pressure anatexis (Mount Stafford, central Australia). *Journal of Petrology*, *47*, 1973–1996. https://doi.org/10.1093/petrology/egl033

Seydoux-Guillaume, A. M., Wirth, R., Heinrich, W., & Montel, J. M. (2002). Experimental determination of Thorium partitioning between monazite and xenotime using analytical electron microscopy and X-ray diffraction Rietveld analysis. *European Journal of Mineralogy*, *14*, 869–878. https://doi.org/10.1127/0935-1221/2002/0014-0869

Spear, F. S. (2010). Monazite–allanite phase relations in metapelites. *Chemical Geology*, *279*, 55–62. https://doi.org/10.1016/j.chemgeo.2010.10.004

Spear, F. S., & Pyle, J. M. (2010). Theoretical modeling of monazite growth in a low Ca metapelite. *Chemical Geology*, *273*, 111–119. https://doi.org/10.1016/j.chemgeo.2010.02.016

Spencer, K. J., Hacker, B. R., Kylander-Clark, A. R. C., Andersen, T. B., Cottle, J. M., Stearns, M. A., … Seward, G. G. E. (2013). Campaign-style titanite U-Pb dating by laser-ablation ICP: Implications for crustal flow, phase transformations and titanite closure. *Chemical Geology*, *341*, 84–101. https://doi.org/10.1016/j.chemgeo.2012.11.012

Stepanov, A. S., Hermann, J., Rubatto, D., & Rapp, R. P. (2012). Experimental study of monazite/melt partitioning with implications for the REE, Th and U geochemistry of crustal rocks. *Chemical Geology*, *300*, 200–220. https://doi.org/10.1016/j.chemgeo.2012.01.007

Taylor, R. J. M., Clark, C., Harley, S. L., Kylander-Clark, A. R. C., Hacker, B. R., & Kinny, P. D. (2017). Interpreting granulite facies events through rare earth element partitioning arrays. *Journal of Metamorphic Geology*. http://onlinelibrary.wiley.com/doi/10.1111/jmg.12254/full

Van Orman, J. A., Grove, T. L., Shimizu, N., & Layer, G. D. (2002). Rare earth element diffusion in a natural pyrope single crystal at 2.8 GPa. *Contributions to Mineralogy & Petrology*, *142*, 416–424. https://doi.org/10.1007/s004100100304

Walsh, E. O., & Hacker, B. R. (2004). The fate of subducted continental margins: Two-stage exhumation of the high-pressure to ultrahigh-pressure Western Gneiss complex, Norway. *Journal of Metamorphic Geology*, *22*, 671–689. https://doi.org/10.1111/j.1525-1314.2004.00541.x

Warren, C. J., Greenwood, L. V., Argles, T. W., Roberts, N. M., Parrish, R. R., & Harris, N. B. (2018). Garnet–monazite rare earth element relationships in sub-solidus metapelites: A case study from Bhutan. *Geological Society, London, Special Publications*, *478*, SP478.

SUPPORTING INFORMATION

Additional supporting information may be found online in the Supporting Information section at the end of the article.

Table S1. Garnet–monazite partitioning.

How to cite this article: Hacker B, Kylander-Clark A, Holder R. REE partitioning between monazite and garnet: Implications for petrochronology. *J Metamorph Geol*. 2019;37:227–237. https://doi.org/10.1111/jmg.12458